Available online at http://scik.org
Eng. Math. Lett. 2016, 2016:6
ISSN: 2049-9337

A RADIAL BASIS FUNCTION WENO METHOD WITH STENCIL ADAPTIVITY

TERHEMEN ABOIYAR[1,*], MARY-ANNE MSUUR SHIOR[2], DANASABE TAMA ALI[3]

[1]Department of Mathematics/Statistics/Computer Science,University of Agriculture, PMB 2373, Makurdi, Nigeria.

[2]Department of Mathematics and Computer Science,Benue State University, Makurdi, Nigeria.

[3]Taraba State Polytechnic, Suntai, Jalingo Campus, Nigeria.

Copyright © 2016 Aboiyar, Shior, and Ali. This is an open access article distributed under the Creative Commons Attribution License, which permits unrestricted use, distribution, and reproduction in any medium, provided the original work is properly cited.

Abstract. In this paper, the flexibility in the choice of stencil sizes in the radial basis function Weighted Essentially Non-Oscillatory (WENO) reconstruction is used to develop a stencil adaptivity strategy that will be coupled with the WENO method. The size of the stencil is determined by the value of an *a posteriori* error indicator which determines whether the stencil lies in a smooth region of the solution or across a discontinuity. Numerical results are presented for thin plate spline reconstruction to illustrate the benefits of the proposed method.

Keywords: radial basis functions; thin plate splines; finite volume method; triangular meshes; stencil adaptivity

2010 AMS Subject Classification: 65M08.

1. Introduction

High order finite volume methods have become standard methods for the solving hyperbolic conservation laws. In general, the design of these methods consists of two steps. In the first

*Corresponding author

E-mail addresses: t.aboiyar@uam.edu.ng (T. Aboiyar), talk2msuurshior@ymail.com (M.A.M. Shior), a-mawanatama@yahoo.com (D.T. Ali)

Received February 4, 2016

step, known as the reconstruction step, high order polynomials are defined within the control volume from the cell average values of the variables. The second step involves the interface fluxes of the control volume, from which the cell averages of the variables are then obtained for a solution at the next time level [12].

The weighted essentially non-oscillatory (WENO) reconstruction first selects, for each cell of a finite volume discretization, a set of stencils, each comprising a set of neighboring cells. On each stencil, a solution reconstruction is obtained and a weighted sum of the reconstruction functions are used to approximate the solution over a control volume of the finite volume discretization. The required weights are determined by using an appropriate oscillation indicator. WENO schemes were first formulated by [5, 7, 8, 11]. All these reconstructions were based on polynomials.

It was observed in the numerical experiments in [1] that polynomial reconstruction schemes may lead to numerical instability. To this end, Aboiyar *et al* [2] proposed WENO reconstructions over conforming unstructured triangulations using polyharmonic splines rather than polynomials. Polyharmonic splines, a class of radial basis functions (RBFs), were shown to yield numerically stable interpolants. The authors observed that WENO reconstruction by polyharmonic splines is, in comparison with polynomial reconstruction not only more stable, but also more flexible. More precisely, the stencil selection procedure is more flexible in the polyharmonic spline reconstruction. In polynomial reconstruction, the size of the stencil is determined by the degree of the polynomial interpolant. In contrast, the polyharmonic spline reconstruction scheme is much less restrictive, when it comes to the selection of the individual stencils and their sizes. In this paper, we utilize the additional freedom in the choice of stencil size to adapt the size of the stencils depending on whether the stencil crosses a discontinuity or not during simulation. We refer to this technique as *stencil adaptivity*.

The rest of the paper is organized as follows. In section 2, we will briefly review the radial basis function WENO method of Aboiyar *et al* [2] in section 3, we will describe the proposed stencil adaptivity method while in section 4 we will couple stencil adaptivity with mesh adaptivity. Finally, we draw some conclusions in section 5.

2. Methodology

0.1. **A review of the radial basis function WENO method.** The WENO method in this paper is based on a finite volume discretization for the two dimensional conservation law

$$\frac{\partial u}{\partial t} + \nabla \cdot f(u) = 0, \tag{1}$$

on a unstructured conforming triangulation $\mathscr{T}$ of a computational domain $\Omega \in \mathbb{R}^2$ subject to appropriate initial and boundary conditions. The function $f(u) = (f_1(u), f_2(u))^T$ is known as the flux function.

For any triangle $T \in \mathscr{T}$, the semi-discrete scheme, based on the integral form of (1), has the form

$$\frac{d}{dt}\bar{u}_T(t) + \frac{1}{|T|}\int_{\partial T} f(u)\cdot \mathbf{n}\, ds = 0, \qquad \text{for } T \in \mathscr{T}, \tag{2}$$

where $\bar{u}_T$ denotes the cell average of u over triangle $T \in \mathscr{T}$ at time $t \in I$, $\mathbf{n}$ is the outward unit normal vector of the triangle's boundary ∂T and $|T|$ is the area of triangle T. The line integral in (2) can be discretized using a p-point Gaussian integration formula the Lax-Friedrichs numerical flux function can be used to approximate the flux across the boundary of neighboring triangles to $T \in \mathscr{T}$.

To maintain stability, time stepping is done with the third order strong stability preserving Runge-Kutta method of [13]. This method is known in the earlier literature as the Total Variation Diminishing (TVD) Runge-Kutta method. Further details on the finite volume method can be found in [10].

To obtain a finite volume method that is high order in space, a solution reconstruction has to be obtained on each cell of the finite volume discretization. We will now show how radial basis functions can be used for this purpose.

Given a conforming triangulation $\mathscr{T} = \{T\}_{T\in\mathscr{T}}$ and a triangle $T \in \mathscr{T}$, we consider a stencil

$$\mathscr{S} = \{T_1, T_2, \ldots, T_n\} \subset \mathscr{T}$$

of size n, containing T. Given the cell averages $\{\bar{u}_T\}_{T\in\mathscr{S}}$ for any stencil $\mathscr{S} \subset \mathscr{T}$, we solve the reconstruction problem

$$\lambda_T(s) = \bar{u}_T, \qquad \text{for all } T \in \mathscr{S}, \tag{3}$$

where

$$s(\mathbf{x}) = \sum_{T\in\mathscr{S}} c_T \lambda_T^y \phi(\|\mathbf{x}-\mathbf{y}\|) + p(\mathbf{x}), \qquad p \in \mathscr{P}_m^d, \tag{4}$$

is the form of the reconstruction s. Moreover, $\phi : [0,\infty) \to \mathbb{R}$ as a fixed radial function, $\|\cdot\|$ is the Euclidean norm on $\mathbb{R}^d$ and λ_T is the cell average operator on T. Furthermore, $\mathscr{P}_m^d$ is defined as the vector space of all d-variate polynomials of degree at most $m-1$ with dimension of $\mathscr{P}_m^d$ is $q = \dim(\mathscr{P}_m^d) = \binom{m-1+d}{d}$. We also note that

$$\lambda_T^y \phi(\|\mathbf{x}-\mathbf{y}\|) = \frac{1}{|T|}\int_T \phi(\|\mathbf{x}-\mathbf{y}\|)\, d\mathbf{y}.$$

Examples of RBFs can be found in [4, 15].

The reconstruction s in (4) contains $n+q$ parameters, but at only $n = \#\mathscr{S}$ interpolation conditions in (3). To obtain the addition q parameters, we need to solve (3) under the side conditions

$$\sum_{T\in\mathscr{S}} c_T \lambda_T(p) = 0, \qquad \text{for all} \quad p \in \mathscr{P}_m^d. \tag{5}$$

This leads us to the $(n+q)\times(n+q)$ linear system

$$\begin{bmatrix} A & P \\ P^T & \mathbf{0} \end{bmatrix} \begin{bmatrix} \mathbf{c} \\ \mathbf{d} \end{bmatrix} = \begin{bmatrix} \bar{u}_{\mathscr{S}} \\ 0 \end{bmatrix}, \tag{6}$$

where

$$A = (\lambda_T^x \lambda_R^y \phi(\|\mathbf{x}-\mathbf{y}\|))_{T,R\in\mathscr{S}} \in \mathbb{R}^{n\times n} \text{ and } P = (\lambda_T(\mathbf{x}^\alpha))_{T\in\mathscr{S},0\le|\alpha|<m} \in \mathbb{R}^{n\times q},$$

and $\bar{u}_{\mathscr{S}} = (\bar{u}_T)_{T\in\mathscr{S}} \in \mathbb{R}^n$.

When using polyharmonic splines, the radial function $\phi \equiv \phi_{d,k}$ is,for $d,k \in \mathbb{N}$ with $2k > d$, given by

$$\phi_{d,k}(r) = \begin{cases} r^{2k-d} & \text{for } d \text{ odd;} \\ r^{2k-d}\log(r) & \text{for } d \text{ even;} \end{cases}$$

where d denotes the space dimension and k is the order of the basis function $\phi_{d,k}$. Our emphasis in this paper is the case $d = k = 2$ which is the thin plate spline with $\phi_{2,2}(r) = r^2\log(r)$. In this case, the reconstruction s in (4) has the form

$$s(\mathbf{x}) = \sum_{T\in\mathscr{S}} c_T \lambda_T^y \left(\|\mathbf{x}-\mathbf{y}\|^2 \log(\|\mathbf{x}-\mathbf{y}\|)\right) + d_1 + d_2 x_1 + d_3 x_2,$$

where $\mathbf{x} = (x_1, x_2)^T \in \mathbb{R}^2$. The polyharmonic splines possesses an optimal reconstruction property in the Beppo-Levi space [15].

The WENO reconstruction method computes a recovery function s_i on a number of stencils $\mathscr{S}_i$ for a cell T and then uses a weighted sum:

$$s := \sum_i \omega_i s_i$$

of the recovery functions where

$$\omega_i = \frac{(\varepsilon + \mathscr{I}(s_i))^{-\rho}}{\sum_j (\varepsilon + \mathscr{I}(s_j))^{-\rho}}, \qquad \varepsilon, \rho > 0.$$

and $\mathscr{I}(s_i)$ is the oscillation indicator of s_i. The positive weights ω_i with $\sum_i \omega_i = 1$ are chosen in such a way that ω_i is small if the oscillation of s_i is high, reflecting the fact that the stencil lies in a region where the solution is subject to strong variation, and ω_i is larger for less oscillating s_i, i.e. the stencil $\mathscr{S}_i$ lies in regions where the solution is smooth.

We note that the solution of (6) consists of $n+q$ conditions, where we require $n > q$ for the well-posedness of the reconstruction problem (4), (5). But otherwise, there is no further restriction on the stencil size. However in polynomial reconstruction, the number of cells in any stencil is determined by the chosen degree of the polynomial space. This restriction is regarded as a serious disadvantage of the polynomial reconstruction scheme as it may be difficult to find the exact degrees of freedom especially in unstructured grids. On the other hand, the polyharmonic spline reconstruction scheme is much less restrictive when it comes to the selection of the individual stencils and their sizes. Indeed, the additional freedom allows for flexibility in the choice of stencil size and this forms the basis for our proposed method.

0.2. **Stencil adaptivity.**

0.2.1. *The error indicator.* The design and implementation of any adaptive method is usually guided by a suitable error indicator. An error indicator is normally computed for each cell $T \in \mathscr{T}$ and used to detect if a cell lies in a region where the approximation error is large.

Following [9, 3], we will use thin plate spline interpolation will be used in computing an error indicator for each triangle of a triangulation $\mathscr{T}$. In order to compute this error indicator,

we first of all assume that each cell average value $\bar{u}_T$, $T \in \mathscr{T}$ is assigned to the barycenter $\mathbf{b}_T$ of the cell T, i.e. $\bar{u}_T \equiv \bar{u}(\mathbf{b}_T)$. We then compute a thin plate spline interpolant s of the form

$$s(\mathbf{x}) = \sum_{T' \in \mathscr{N}_{\mathrm{M}}(T)} c_{T'} \|\mathbf{x} - \mathbf{b}_{T'}\|^2 \log \|\mathbf{x} - \mathbf{b}_{T'}\| + p(\mathbf{x}), \qquad p \in \mathscr{P}_k^2, \tag{7}$$

where the barycenters $\mathbf{b}_{T'}$ of the triangles in the Moore neighborhood $\mathscr{N}_{\mathrm{M}}(T)$ of T are regarded as the interpolation points, i.e. s satisfies the interpolation condition

$$s(\mathbf{b}_{T'}) = \bar{u}(\mathbf{b}_{T'}) \quad \text{for all} \quad T' \in \mathscr{N}_{\mathrm{M}}(T).$$

Recall that the Moore neighborhood of a cell $T \in \mathscr{T}$ contains all cells in $\mathscr{T}$ which are sharing a common edge or a common vertex with T. Note that the Moore neighborhood $\mathscr{N}_{\mathrm{M}}(T)$ of T does not contain T. The error indicator is then defined as

$$\varepsilon_T = |\bar{u}(\mathbf{b}_T) - s(\mathbf{b}_T)|. \tag{8}$$

Therefore, the error indicator $\varepsilon : \mathscr{T} \mapsto \mathbb{R}$ estimates the local approximation behaviour in the neighborhood of each triangle in $\mathscr{T}(t)$. A large value of ε_T indicates a large approximation error around T, while a small value of ε_T indicates a small approximation error around T.

0.2.2. *The method.* We have highlighted the flexibility available in the stencil selection algorithm in the polyharmonic spline reconstruction method. In fact, we only have a lower bound for the stencil size so as to obtain non-trivial recovery. There is actually no upper bound for the stencil size, although for the sake of computational cost we generally try to keep it relatively small [14]. We can use this flexibility in stencil selection to adaptively adjust the size of the stencil used for recovery on different cells of the finite volume method during the simulation.

After extensive numerical tests, we observed that for reconstruction with thin plate splines, seven stencils of size four were most suitable and gave very good approximations for problems where the solution was smooth everywhere at all times. This required us to solve a 7×7 linear system for each stencil. On the other hand, when we treated problems with discontinuities or steep slopes in the solution, seven stencils of size seven were preferred because we were able to get stencils where the interpolant was non-oscillatory. To this end, we propose a simple stencil adaptivity strategy on the basis of the size of the error indicator ε_T as follows: *Suppose* $\varepsilon^* = \max_{T \in \mathscr{T}} \varepsilon_T$*, and let* ϑ *be a threshold value satisfying* $0 < \vartheta < 1$*. On cells with* $\varepsilon_T > \vartheta \cdot \varepsilon^*$*,*

we use stencils of size seven for the thin plate spline WENO reconstruction otherwise we use stencils of size four. In the numerical experiments in this section, we will use $\vartheta = 0.05$.

We will use the stencil adaptivity in the WENO reconstruction to solve the linear advection equation and Burgers' equation and compare the results with those obtained when fixed stencil sizes were used.

3. Results and Discussion

0.3. **Example: Linear advection.** We solve the linear advection equation

$$u_t + u_{x_1} + u_{x_2} = 0, \quad \text{for } u \equiv u(t,\mathbf{x}) \quad \text{with} \quad \mathbf{x} = (x_1, x_2) \in \mathbb{R}^2, \tag{9}$$

with initial data[6]

$$u_0(\mathbf{x}) = \begin{cases} \exp\left(\frac{\|\mathbf{x}-\mathbf{c}\|^2}{\|\mathbf{x}-\mathbf{c}\|^2 - R^2}\right), & \|\mathbf{x}-\mathbf{c}\| < R; \\ 0, & \text{otherwise}, \end{cases} \tag{10}$$

with $R = 0.15$, $\mathbf{c} = (-0.2, -0.2)^{\mathrm{T}}$ on the computational domain $\Omega = [-0.5, 0.5] \times [-0.5, 0.5] \subset \mathbb{R}^2$ using the thin plate spline WENO method. The WENO reconstruction is implemented with both stencil adaptivity and fixed stencil sizes and we show the errors in the L_1-, L_2- and L_∞-norms at time $t = 0.25$ on meshes of sizes $h = \frac{1}{16}$, $h = \frac{1}{32}$ and $h = \frac{1}{64}$ with 512, 2048 and 8192 triangles respectively.

TABLE 1. Solution of (9), (10) on fixed stencil sizes.

h	E_1	E_2	E_∞	N_4	N_7
$1/16$	$2.0122 \cdot 10^{-2}$	$6.1310 \cdot 10^{-2}$	$3.6325 \cdot 10^{-1}$	–	512
$1/32$	$7.9146 \cdot 10^{-3}$	$2.6562 \cdot 10^{-2}$	$1.9183 \cdot 10^{-1}$	–	2048
$1/64$	$2.3427 \cdot 10^{-3}$	$1.0529 \cdot 10^{-2}$	$8.0493 \cdot 10^{-2}$	–	8192

We see from Table 1, which shows the results at $t = 0.25$, that there is little difference in the errors when we use fixed stencil sizes and when we use variable stencil sizes. In fact, we observed a slight improvement when stencil adaptivity was used. However, we significantly reduce the computational time by using smaller stencils on a large number of cells. Note that in

TABLE 2. Solution of (9), (10) on adapted stencils.

h	E_1	E_2	E_∞	N_4	N_7
$1/16$	$1.9748 \cdot 10^{-2}$	$6.0187 \cdot 10^{-2}$	$3.6077 \cdot 10^{-1}$	433	79
$1/32$	$7.4548 \cdot 10^{-3}$	$2.5282 \cdot 10^{-2}$	$1.5023 \cdot 10^{-1}$	1858	190
$1/64$	$1.8588 \cdot 10^{-3}$	$8.2181 \cdot 10^{-3}$	$8.0328 \cdot 10^{-2}$	7456	736

this paper, N_4 denotes the number of cells where stencils of size four were used for reconstruction while N_7 denotes the number of cells where stencils of size seven were used. In addition, E_1, E_2 and E_∞ denote the errors in the L_1-, L_2- and L_∞-norms respectively.

0.4. **Example: Burgers' equation.** We further demonstrate the benefits of stencil adaptivity by solving Burgers' equation

$$u_t + \left(\frac{1}{2}u^2\right)_{x_1} + \left(\frac{1}{2}u^2\right)_{x_2} = 0, \tag{11}$$

with initial condition (10) on the computational domain $\Omega = [-0.5, 0.5] \times [-0.5, 0.5] \subset \mathbb{R}^2$. We solve this problem using stencil adaptation on fixed meshes with mesh widths $h = \frac{1}{16}$, $h = \frac{1}{32}$ and $h = \frac{1}{64}$ and also using fixed stencil sizes. The simulation is run until time $t = 1.2$.

TABLE 3. Solution of (11), (10) on fixed stencil sizes.

h	E_1	E_2	E_∞	N_4	N_7
$1/16$	$1.2415 \cdot 10^{-2}$	$4.4681 \cdot 10^{-2}$	$4.2769 \cdot 10^{-1}$	–	512
$1/32$	$7.1652 \cdot 10^{-3}$	$3.3673 \cdot 10^{-2}$	$2.1775 \cdot 10^{-1}$	–	2048
$1/64$	$2.2880 \cdot 10^{-3}$	$1.6900 \cdot 10^{-2}$	$8.2838 \cdot 10^{-2}$	–	8192

TABLE 4. Solution of (11), (10) on fixed stencil sizes.

h	E_1	E_2	E_∞	N_4	N_7
$1/16$	$1.2318 \cdot 10^{-2}$	$4.4558 \cdot 10^{-2}$	$4.2726 \cdot 10^{-1}$	445	67
$1/32$	$7.0508 \cdot 10^{-3}$	$3.3647 \cdot 10^{-2}$	$2.1631 \cdot 10^{-1}$	1940	108
$1/64$	$1.8733 \cdot 10^{-3}$	$1.4550 \cdot 10^{-2}$	$8.2533 \cdot 10^{-2}$	7625	567

We once again see from Tables 2 and 3 that there is little difference in the errors when fixed stencil sizes are used and when variable stencil sizes are used. Thus, we see that for both the

linear advection equation and Burgers' equation, stencil adaptivity does not affect the accuracy of the solution.Figure 1(a) shows the distribution of the stencil sizes for the various cells at time $t = 1.2$ on the mesh of width $h = \frac{1}{32}$. The cells in the dark area are those where stencils of size seven were used for the WENO reconstruction, while the white ones are those where stencils of size four were used for the reconstruction.

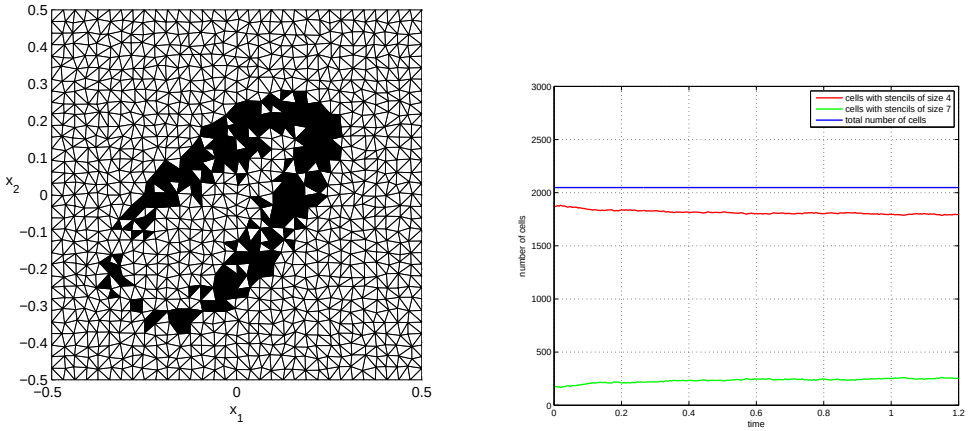

(a) (b)

FIGURE 1. (a) Stencil size distribution and (b) number of cells with particular stencil size.

From Figure 1(b), which shows the distribution of the stencil sizes throughout the simulation, we notice a slight but steady increase in the number of cells where the reconstruction was done with stencils of size seven as the simulation advances in time. This is because of the increasing support of the solution, which is due to the nonlinearity of the Burgers' equation. This means that there is also a growth in the length of the shock front. In any case, throughout the simulation, the reconstruction of over 80% of the cells was done with stencils of size four, and this can significantly reduce the simulation time.

0.5. **Mesh & stencil Adaptivity.** We seek further reduction in computational cost by combining the mesh adaptivity algorithm of [9, 3] with stencil adaptivity for the WENO method using thin plate spline reconstruction. To accomplish this, we use the same indicator (8) for both mesh adaptivity and stencil adaptivity. The strategy we use in marking cells for refining or coarsening (mesh adaptivity) is summarized as follows: *Let* $\varepsilon^* = \max_{T\in\mathscr{T}} \varepsilon_T$*, and let* ϑ_r, ϑ_d *be two*

threshold values satisfying $0 < \vartheta_{\mathrm{d}} < \vartheta_{\mathrm{r}} < 1$. *We say that a cell* $T \in \mathscr{T}$ *is to be refined if and only if* $\varepsilon_T > \vartheta_{\mathrm{r}} \cdot \varepsilon^*$, *and* T *is coarsened or derefined if and only if* $\varepsilon_T < \vartheta_{\mathrm{d}} \cdot \varepsilon^*$.

A triangular cell $T \in \mathscr{T}$ is refined by inserting its barycenter $\mathbf{b}_T$ as a new node of the triangulation $\mathscr{T}$. A cell $T \in \mathscr{T}$ is derefined by removing its nodes from the triangulation $\mathscr{T}$. This means that all cells sharing a node have to be marked for derefinement for the node to be successfully removed from the triangulation. At each time step, after all the new nodes have been inserted and the nodes of the triangles to be coarsened have been removed, the triangulation $\mathscr{T}$ is then updated by a local Delaunay re-triangulation. This enables an adaptive modification of the current triangulation $\mathscr{T}(t)$ yielding a modified triangulation $\mathscr{T}(t+\Delta t)$ at the next time step.

In mesh & stencil adaptivity, we require three threshold values ϑ, ϑ_{r} and ϑ_{d}. For stencil adaptivity, we will use stencils of size four for reconstruction on a cell T if $\varepsilon_T \leq \vartheta \cdot \varepsilon^*$ and stencils of size seven if $\varepsilon_T > \vartheta \cdot \varepsilon^*$ where we set $\vartheta = 0.035$. For mesh adaptivity, we set $\vartheta_{\mathrm{r}} = 0.05$ and $\vartheta_{\mathrm{d}} = 0.01$. From our numerical tests, we observed that using $\vartheta < \vartheta_{\mathrm{r}}$ gave better results. We note that mesh adaptivity is performed for stencil adaptivity at each time step. We

TABLE 5. Comparing mesh adaptivity and mesh & stencil adaptivity for the linear advection equation.

method	E_1	E_2	E_∞	N_4	N_7
mesh adaptivity	$2.9060 \cdot 10^{-3}$	$1.0821 \cdot 10^{-2}$	$8.3975 \cdot 10^{-2}$	-	1480
mesh & stencil adaptivity	$2.8926 \cdot 10^{-3}$	$1.0618 \cdot 10^{-2}$	$8.2410 \cdot 10^{-2}$	1018	474

demonstrate the benefits of this combination by solving the linear advection equation (9) with initial data (10) and show the results at $t = 0.25$ for both mesh adaptivity and mesh & stencil adaptivity in Table 3. At the end of our simulation, 1480 cells were used for mesh adaptivity and 1492 cells were used for mesh & stencil adaptivity. We noticed a reduction in computational time for mesh & stencil adaptivity because reconstruction with stencils of size seven was only applied to 474 cells. The number of cells used in the simulation along with the distribution of stencil sizes for mesh & stencil adaptivity are shown in Figure 2(b).

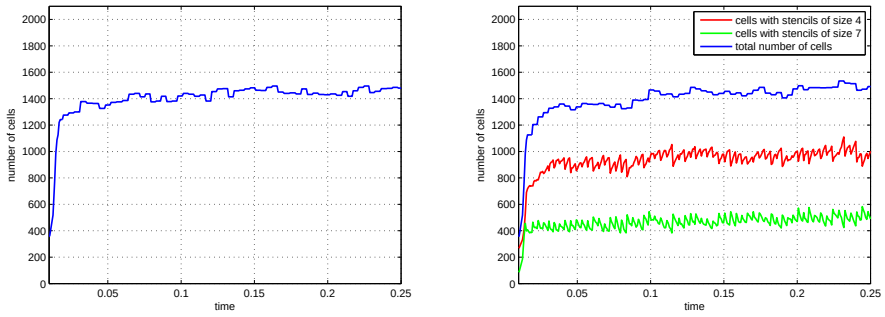

(a) (b)

FIGURE 2. (a) Number of cells for mesh adaptivity and (b) number of cells and stencil size distribution for mesh & stencil adaptivity for the linear advection equation.

We will also use the mesh & stencil adaptivity to solve Burgers' equation (11) with initial data (10) and display the results at $t = 1.2$ for both mesh adaptivity and mesh & stencil adaptivity in Table 4.

TABLE 6. Comparing mesh adaptivity and mesh & stencil adaptivity for Burgers' equation.

method	E_1	E_2	E_∞	N_4	N_7
mesh adaptivity	$1.6848 \cdot 10^{-3}$	$1.1745 \cdot 10^{-2}$	$7.8050 \cdot 10^{-2}$	-	1762
mesh & stencil adaptivity	$1.6702 \cdot 10^{-3}$	$1.1152 \cdot 10^{-2}$	$7.7832 \cdot 10^{-2}$	1112	574

The number of cells used in the simulation along with the distribution of stencil sizes for mesh & stencil adaptivity are shown in Figure 3(b). The adapted mesh and solution at time $t = 1.2$ is shown in Figure 4.

At the end of the simulation, 1762 cells were used for mesh adaptivity while just 1686 cells were used for mesh & stencil adaptivity. We noticed a reduction in computational time when mesh & stencil adaptivity is implemented because reconstruction with stencils of size seven was only applied to 574 cells. A significant advantage of the mesh & stencil adaptivity lies in the fact that the stencil adaptivity step does not require any extra computation of the error indicators since the same error indicator is used for both the mesh adaptivity and stencil adaptivity steps.

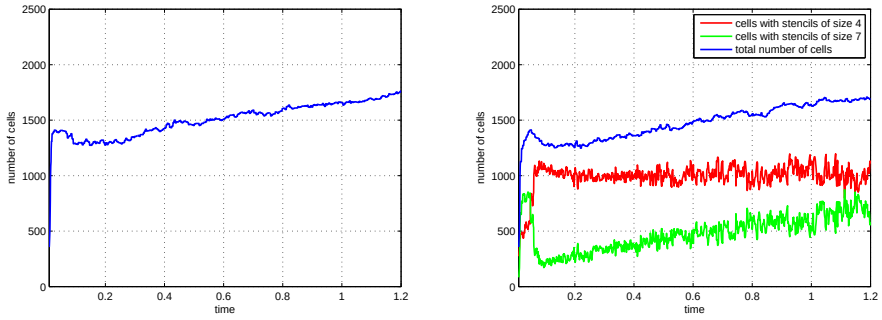

(a) (b)

FIGURE 3. (a) Number of cells for mesh adaptivity and (b) number of cells and stencil size distribution for mesh & stencil adaptivity for Burgers' equation.

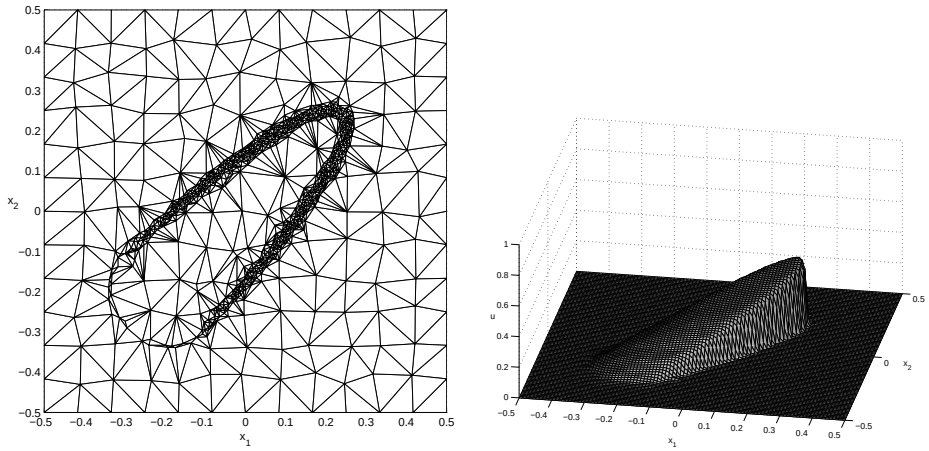

(a) (b)

FIGURE 4. (a) Adapted mesh and 3D plot for Burgers Equation at time $t = 1.2$.

Finally, as displayed in Table 5.4, there is little difference in the errors and so for the sake of computational cost, we believe that coupling mesh adaptivity and stencil adaptivity is very useful in practice.

4. Conclusion

We have proposed a stencil adaptivity procedure to be coupled with the polyharmonic spline WENO reconstruction. We have also included mesh adaptivity in the proposed method.This method can be of high order and is also flexible. The flexibility in the choice of stencil sizes

makes the method particularly attractive. The mesh adaptation procedure also enables the efficient resolution of gradients and shock fronts. The efficiency of the method was also demonstrated with numerical examples.

Conflict of Interests

The authors declare that there is no conflict of interests.

REFERENCES

[1] R. Abgrall, *On ENO schemes on unstructured meshes: analysis and implementation*, J. Comp. Phys., **114** (1994),45 – 58.

[2] T. Aboiyar, E. H. Georgoulis and A. Iske, *High order finite volume schemes using polyharmonic spline reconstruction*, Proceedings of the Intl. Conference on Numerical Analysis and Approximation Theory, Cluj-Napoca, Romania (2006), 113–126.

[3] T. Aboiyar, E. H. Georgoulis and A. Iske, *Adaptive ADER Methods Using Kernel-Based Polyharmonic Spline WENO Reconstruction*, SIAM Journal on Scientific Computing, **32** (2010), 3251–3277.

[4] G. E. Fasshauer, *Meshfree Approximation Methods in MATLAB*, World Scientific (2007).

[5] O. Friedrich, *Weighted essentially non-oscillatory schemes for the interpolation of mean values on unstructured grids*, J. Comp. Phys. , **144** (1998), 194 – 212.

[6] J. Fürst and T. Sonar, *On meshless collocation approximations of conservation laws: positive schemes and dissipation models*, ZAMM, **81** (2001), 403 – 415.

[7] C. Hu and C. W. Shu, *Weighted essentially non-oscillatory schemes on traingular meshes*, J. Comp. Phys., **114** (1999),97 – 127.

[8] G. S. Jiang and C. W. Shu, *Efficient implementation of weighted ENO schemes*, J. Comp. Phys., **126** (1996),202 – 228.

[9] M. Käser and A. Iske, *ADER schemes on adaptive triangular meshes for scalar conservation laws*, J. Comp. Phys, **205** (2005), 486 – 508.

[10] R. J. Leveque, *Finite Volume Methods for Hyperbolic Problems*, Cambridge University Press (2002).

[11] X. Liu, S. Osher and T. Chan, *Weighted essentially non-oscillatory schemes*, J. Comp. Phys., **115** (1994), 200 – 212.

[12] Y. Liu, C. W. Shu, E. Tadmor and M. Zhang, *Non-oscillatory heirarchical reconstructions for central and finite volume schemes*, Comm. Comp. Phys. **2** (2007), 933 – 963.

[13] C. W. Shu and S. Osher, *Efficient implementation of essentially non-oscillatory shock capturing schemes*, J. Comp. Phys., **77**, 439 – 471.

[14] T. Sonar, *Optimal recovery using thin plate splines in finite volume methods for the numerical solution of hyperbolic conservation laws*, IMA J. Num. Anal., **16** (1996), 549 – 581.

[15] H. Wendland, *Scattered Data Approximation*, Cambridge University Press, 2005.